

RESEARCH ARTICLE

# Full characterization of photovoltaic modules in real operating conditions: theoretical model, measurement method, and results

Marco Pierro, Francesco Bucci and Cristina Cornaro\*

Department of Enterprise Engineering, Centre for Hybrid and Organic Solar Energy (CHOSE), University of Rome "Tor Vergata", Via del Politecnico 1, 00133 Rome, Italy

## ABSTRACT

The photovoltaic (PV) system performance essentially depends on the modules response to five effects: spectral, reflection, temperature, irradiance, and nominal power variations. Providing a full characterization of modules behavior in terms of the impact of these effects on real operating conditions performance is very important both to compare different PV technologies and to choose the best technology for a specific site, position, and installation feature. In this work, a systematic approach is used. A theoretical model to calculate the performance ratio related to each effect is proposed. The model is used to compare and to explain the annual behavior of two different technologies modules: mc-Si (KC125) and a-Si/DJ (EPV50). The basic features of these modules performance are observed. Copyright © 2013 John Wiley & Sons, Ltd.

## KEYWORDS

crystalline silicon; amorphous silicon; outdoor monitoring; PV modeling; PV modules; PV performance

## \*Correspondence

Cristina Cornaro, Department of Enterprise Engineering, Centre for Hybrid and Organic Solar Energy (CHOSE), University of Rome "Tor Vergata", Via del Politecnico 1, 00133 Rome, Italy.

E-mail: cornaro@uniroma2.it

Received 26 February 2013; Revised 31 October 2013; Accepted 5 November 2013

## 1. INTRODUCTION

It is well known that the nominal module efficiency ( $\eta_{stc}$ ) cannot give any indication on the photovoltaic (PV) module's behavior in real operating conditions (ROCs) because it is measured in the laboratory at standard test condition (STC). The most used indicator to describe the PV modules outdoor performance is the "performance ratio" (PR) that is the ratio between the efficiency in ROC and the nominal efficiency:  $PR = \eta_{roc}/\eta_{stc}$ .

Performance ratio takes into account all the effects that cause the efficiency variation when the modules do not operate at STC:

- (1) "Spectral effect" that considers the module performance variations that occur when the plane of array (POA) irradiance spectrum is different from  $AM_0 = 1.5G$ .
- (2) "Reflection effect" that considers the module performance losses due to the angle of incident different from  $\theta_0 = 0$ .

- (3) "Temperature effect" that takes into account the changing in electrical behavior of the module that occurs when the cell temperature differs from  $T_0 = 25^\circ\text{C}$ .
- (4) "Irradiance effect" that takes into account the module performance loss that occurs when the POA irradiance intensity differs from  $G_0 = 1000\text{ W/m}^2$ .
- (5) "Nominal power variation effect" that considers the variation of the nominal power measured in a particular day ( $P_{m0}(day)$ ) with respect to the nominal power declared by the module manufacturer ( $P_n$ ). This effect includes possible errors in nominal power measurement, possible initial or long term maximum power degradation, and seasonal power variation.

The PV system performance with respect to modules technology, plant location (site), positioning (tilt and orientation), and installation features (building integration or retrofit) essentially depends on the modules response to these effects. Thus, providing a full characterization of modules behavior in terms of the impact of these effects

on ROC performance is very important both to compare different PV technologies and to choose the best technology for a specific site, position, and installation choice. Nevertheless, in ROC, such effects act simultaneously and, often, in a competitive way so that it is very difficult to recognize and quantify the contribution of each phenomenon to the PR.

In [1] and [2], a review of the most used methods for efficiency and power modeling with respect to temperature and irradiance effects is reported. One of the most used and exhaustive methods for PV performance characterization is the one developed by King *et al.* at the Sandia Laboratory [3,4]. In this model, all the aforementioned effects are described by parametric functions of the climatic variables, but no “nominal power variation effect” is considered, so that the amorphous thin film performance is scarcely reproducible. Besides, the model used to evaluate the spectral effect could be correctly used only for clear sky days because it does not take into account the module spectral response in overcast conditions [5]. More recently, an important contribution to the full characterization of the amorphous thin film performance was reported in the work of Fanni *et al.* [6]. Here, all the main phenomena that affect the a-Si modules performance are measured and modelled, although a complete mathematical description of the model is not reported. However, also in this case, it could be applied to reproduce daily module performance only in clear sky conditions.

In this work, a rigorous approach is used, and the overall PR is described in terms of the product of different PRs. Each PR describes an effect and is calculated by a parametric function of the environmental variables and time. All the model parameters are measured using outdoor data, and a good agreement with the Sandia and other laboratories measurements is found. A modification of the King model to describe the spectral response is proposed, so that it could be applied also in overcast conditions. As a first approach, the nominal power variation effect is described only by an empirical function of time and not explicit dependence from the cumulative radiation energy, and the cell temperature is pointed out. However, the model is able to reproduce the daily performance with a correlation between measured and calculated data of 95% for crystalline module and 67% for the amorphous one. Thus, it is possible to separate and quantify each effect impact on the module efficiency, and a complete characterization of module behavior in ROC is achieved.

The model is used to compare and explain the annual behavior of two different technology modules: mc-Si (KC125) and a-Si/DJ (EPV50). The main features of these modules performance are observed and discussed.

In Section 2, the theoretical model is described. In Section 3, the measurement of each effect and the model parameters values, both for crystalline and amorphous modules, are reported. Agreement between the measured and calculated performance is pointed out. To confirm the reliability of the proposed PR model, a comparison with the King model [3,4] is also reported. For each

phenomenon, the different behavior between the two technologies is discussed.

In Section 4, using 1-year data measurements in ROC, the calculated and measured PRs are compared. The daily performance of the modules is analyzed. Each effect is discussed in detail to explain the seasonal PR behavior. The soiling effect has not been included in the model because the modules have been periodically cleaned, and thus, this effect could be neglected. It should be remarked that the analysis of losses is valid only for the specific ROC. In particular, the reflection loss is very different from a rooftop installation, because each month the module tilt has been changed to maximize the produced energy.

## 2. THEORETICAL MODEL DESCRIPTION

The instantaneous PR depends on the irradiance intensity incident on POA ( $G_i$ ), the irradiance spectrum ( $AM$ ), the angle of incidence ( $\theta$ ), the cell temperature ( $T_{cell}$ ), the nominal power measured in a specific day ( $day$ ) with respect to the nominal power declared by the module manufacturer.

The aim of the model is to express the PR as

$$PR(G_i, AM, \theta, T_{cell}, day) = PR_{am} PR_{aoi} PR_t PR_g \Delta P_n PR_s \quad (1)$$

where  $PR_{am}(G_i, AM, \theta_0, T_0)$  describes the spectral effect,  $PR_{aoi}(G_0, AM_0, \theta, T_0)$  describes the reflection effect,  $PR_t(G_0, AM_0, \theta_0, T_{cell})$  describes the temperature effect,  $PR_g(G_i, AM_0, \theta_0, T_0)$  describes the irradiance effect, and  $\Delta P_n PR_s(day)$  describes the nominal power variation.

In this way, it is possible to isolate each single effect, to study its time behavior, and to quantify its impact on the overall PR.

In the following sections, the models of the single PR contributions are described.

### 2.1. Optical effects

The optical effects are related to the features of the incident irradiance (spectrum and angle of incidence) and depend on the spectral response of the module and on the optical transmittance of the glass (or transparent module protection packaging).

In the first approximation, for small series resistance and big shunt resistance, the short circuit current ( $I_{sc}$ ) is almost equal to the photogenerated current ( $I_{ph}$ ) that is proportional to the POA irradiance transmitted by the glass and absorbed by the cells ( $G_i^{\alpha\tau}$ ).

So, at a fixed cell temperature,  $T_{cell} = T_0$ , it is possible to write

$$I_{sc} \simeq I_{ph} = \cos \theta G_i^{\alpha\tau} = \frac{I_{sc0}}{G_0} G_i^{\alpha\tau} \quad (2)$$

where  $I_{sc0}$  is the short circuit current at STC.

Neglecting the irradiance absorbed by the glass and the irradiance reflected by the cells, it is possible to write Equation 2 as

$$Isc(G_i, AM, \theta_0, T_0) \simeq Isc_0 \frac{G_i}{G_0} \frac{G_i^{\alpha\tau}}{G_i^\tau} \frac{G_i^\tau}{G_i} = Isc_0 \frac{G_i}{G_0} PR_{am}(AM) PR_{aoi}(\theta) \quad (3)$$

where  $G_i^\tau$  is the irradiance transmitted by the glass that reaches the cells.

**2.1.1. Spectral effect.**

At  $\theta = \theta_0$ , the optical transmittance of the glass is almost equal to 1, so

$$G_i^\tau \simeq G_i = \int_0^\infty SR_{pir}(\lambda) \Phi_{am}(\lambda) d\lambda \quad (4)$$

$$G_i^{\alpha\tau} \simeq G_i^\alpha = \int_0^\infty SR_{PV}(\lambda) \Phi_{am}(\lambda) d\lambda$$

$$\times \left[ \frac{\int_0^\infty SR_{pir}(\lambda) \Phi_{am0}(\lambda) d\lambda}{\int_0^\infty SR_{PV}(\lambda) \Phi_{am0}(\lambda) d\lambda} \right] =$$

$$= \int_0^\infty SR_{PV}(\lambda) \Phi_{am}(\lambda) d\lambda \left[ \frac{G_0}{Isc_0} \right]$$

where  $\Phi_{am}$  is the solar spectral irradiance at a fixed AM,  $SR_{pir}$  and  $SR_{PV}$  are the spectral response of the pyranometer (used to measure the irradiance) and the cells, and  $\left[ \frac{G_0}{Isc_0} \right]$  is a corrective factor, measured at  $AM_0 = 1.5G$ , that takes into account the different spectral performance between the cells and the instrument used to measure the incident irradiance (pyranometer).

The solar spectral irradiance (at  $\theta = \theta_0$ ) is the sum of the direct normal spectral irradiance ( $\Phi_{am}^{DNI}$ ) and the POA diffuse spectral irradiance ( $\Phi_{am}^{SH}$ ). The  $\Phi_{am}^{SH}$  does not depend on the air mass but depends on the instantaneous

AQ10 cloud ratio (CR) on POA  $\left( CR_i = \frac{G_i^{sh}}{G_i} = \frac{G_i - G_i^{dni}}{G_i} \right)$ .

In this way, from Equations 3 and 4, it is possible to define

$$PR_{am}(G_i, AM, \theta_0, T_0) = \frac{G_i^{\alpha\tau}}{G_i^\tau} \simeq \frac{G_i^\alpha}{G_i} =$$

$$= \left[ \frac{G_0}{Isc_0} \right]$$

$$\times \frac{\int_0^\infty SR_{PV}(\lambda) \Phi_{am}^{DNI}(\lambda) d\lambda + \int_0^\infty SR_{PV}(\lambda) \Phi_{am}^{SH}(\lambda) d\lambda}{G_i} =$$

$$= \frac{AMM(AM)G_i^d + CRM(CR_i)G_i^{sh}}{G_i}$$

$$= \frac{Isc(G_i, AM, \theta_0, T_0)}{Isc_0 (G_i/G_0)}$$

$$AMM(AM) = \left[ \frac{G_0}{Isc_0} \right] \frac{\int_0^\infty SR_{PV}(\lambda) \Phi_{am}^{DNI}(\lambda) d\lambda}{G_i^d}$$

$$CRM(CR_i) = \left[ \frac{G_0}{Isc_0} \right] \frac{\int_0^\infty SR_{PV}(\lambda) \Phi_{am}^{SH}(\lambda) d\lambda}{G_i^{sh}}$$

where  $G_i$ ,  $G_i^d$ ,  $G_i^{sh}$  are the global, direct, and diffuse irradiance on the POA.

The function  $AMM(AM)$  is the ‘‘air mass modifier’’ and takes into account the module spectral performance to the direct POA irradiance at a fixed  $CR_i$ , while  $CRM(CR_i)$  is the ‘‘cloud ratio modifier’’ and takes into account the module spectral performance to the diffuse POA irradiance at a fixed  $AM \simeq AM_0$ .

It has to be noted that the proposed model is a simplified approach. The main hypothesis is that the irradiance spectrum could be fully described by AM and CR and that the function CRM does not depend on AM. More complete models describe the spectral performance in terms of the spectrum indicator, APE or spectrum and quantum efficiency, UF, as reported in [7–9]. Although it is still not clear how much these approaches improve the spectral effect, description and a detailed comparison between the models should be performed.

The functions  $CRM(CR_i)$  and  $AMM(AM)$  can be approximated as

$$CRM(CR_i) \simeq CA_0 + CA_1(CR_i)$$

$$AMM(AM) \simeq \sum_{n=0}^4 CB_n(AM)^n$$

where the coefficients CA and CB can be calculated from Equation 5, by interpolation of the measured data  $\left( \frac{Isc(G_i, AM, \theta_0, T_0)}{Isc_0(G_i/G_0)} \right)$ .

The air mass is calculated as reported in [4]:

$$AM \simeq \frac{e^{(-.0001184)h}}{\cos(Zs) + 0.5057(96.08 - Zs)^{-1.634}}$$

where Zs is the zenith angle of the sun in degrees and h is the site altitude  $\simeq 100$  m.

It is important to remark that the Sandia model developed by King *et al.* [4] calculates the spectral effect using only Equation 4, and this approximation allows to evaluate the spectral contribution only in clear sky days. Indeed for cloudy days, this effect does not depend on the air mass any more, and the use of the King function,  $f1(AM)$ , leads to an overestimation of the spectral effect impact. With the present approach, it is possible to calculate the spectral contribution for both overcast and clear conditions.

**2.1.2. Reflection effect.**

From Equation 3, it is possible to define

$$\begin{aligned}
 PR_{aoi}(G_0, AM_0, \theta, T_0) &= \frac{G_i^{\tau}}{G_i} = & (6) \\
 &= \frac{\tau^d(\theta)G^{dni} + \tau^{sh}G_i^{sh}}{G_i} \simeq \\
 &\simeq \frac{IAM(\theta)G^{dni} \cos(\theta) + G_i^{sh}}{G_i} = \\
 &= \frac{Isc(G_i, AM_0, \theta, T_0)}{Isc_0(G_i/G_0)PR_{am}} \\
 IAM(\theta) &= \frac{\tau^d(\theta)}{\cos(\theta)}
 \end{aligned}$$

where  $\tau^d(\theta)$  and  $\tau^{sh}$  are the optical transmittance of the glass with respect to the anisotropic direct normal irradiance  $G^{dni}$  and the isotropic diffuse irradiance  $G_i^{sh} = G_i - G^{dni} \cos(\theta)$ . The approximation is possible because  $\tau^{sh}$  does not depend on  $\theta$  ( $G_i^{sh}$  is isotropic irradiation) and almost equal to 1 for any  $\lambda$  belonging to the visible spectrum (the glass is transparent in the visible spectrum).

The function  $IAM(\theta)$  is the ‘‘incident angle modifier’’ and takes into account the variation of the transmitted irradiance when the incident angle is different from  $\theta_0 = 0$ . It can be approximated as [4]

$$IAM(\theta) \simeq \sum_{n=0}^5 CC_n(\theta)^n$$

where the coefficient  $CC$  can be calculated from Equation 6, by interpolation of the measured data  $\frac{Isc(G_i, AM, \theta, T_0)}{Isc_0(G_i/G_0)PR_{am}}$ .

## 2.2. Temperature effect

It is well known that as a first approximation, the main electrical parameters of a solar cell depend linearly on the cell temperature:

$$\begin{aligned}
 Isc(G_0, AM_0, \theta_0, T_{cell}) &= Isc_0 (1 + \alpha \Delta T_{cell}) \\
 Voc(G_0, AM_0, \theta_0, T_{cell}) &= Voc_0 (1 + \beta \Delta T_{cell}) \\
 I_m(G_0, AM_0, \theta_0, T_{cell}) &= Im_0 (1 + \alpha' \Delta T_{cell}) \quad (7) \\
 V_m(G_0, AM_0, \theta_0, T_{cell}) &= Vm_0 (1 + \beta' \Delta T_{cell}) \\
 P_m(G_0, AM_0, \theta_0, T_{cell}) &= Pm_0 (1 + \gamma \Delta T_{cell})
 \end{aligned}$$

where  $\alpha, \alpha', \beta, \beta', \gamma$  are the temperature coefficients expressed in  $1/^\circ\text{C}$ , and  $\Delta T_{cell} = (T_{cell} - 25)^\circ\text{C}$ .

So that it is possible to define

$$PR_t(G_0, AM_0, \theta_0, T_{cell}) = \frac{P_m(G_0, AM_0, \theta_0, T_{cell})}{P_{m0}} = (1 + \gamma \Delta T_{cell}) \quad (8)$$

The STC electrical and temperature coefficients can be calculated from Equation 7, by linear interpolation of the measured data.

## 2.3. Irradiance effect

King *et al.* [4] show that cell current and voltage at the maximum power point can be modeled as

$$V_m(G_i, AM_0, \theta_0, T_0) = \frac{V_m(G_i, AM, \theta, T_0)}{(1 + \beta' \Delta T_{cell})} \simeq \quad (9a)$$

$$\simeq V_{m0} \left( 1 + C_1 \ln \left( \frac{G_i}{G_0} \right) + C_2 \left( \ln \left( \frac{G_i}{G_0} \right) \right)^2 \right)$$

$$I_m(G_i, AM_0, \theta_0, T_0) = \frac{I_m(G_i, AM, \theta, T)}{(1 + \alpha' \Delta T_{cell})PR_{am}PR_{aoi}} \simeq \quad (9b)$$

$$\simeq I_{m0} \left( C_{31} \frac{G_i}{G_0} + C_{32} \left( \frac{G_i}{G_0} \right)^2 \right) \simeq$$

$$\simeq I_{m0} C_3 \left( \frac{G_i}{G_0} \right)$$

The second approximation in Equation 9b is possible because  $C_{31} + C_{32} = 1$  with  $C_{32} \ll 1$ .

From Equations 9a and 9b, it is possible to define

$$\begin{aligned}
 PR_g(G_i, AM_0, \theta_0, T_0) &= \frac{P_m(G_i, AM_0, \theta_0, T_0)}{P_{m0}(G_i/G_0)} = & (10) \\
 &= \left( 1 + C_1 \ln \left( \frac{G_i}{G_0} \right) + C_2 \left( \ln \left( \frac{G_i}{G_0} \right) \right)^2 \right) C_3
 \end{aligned}$$

The coefficients  $C_1, C_2, C_3$  are dimensionless and can be calculated from Equations 9a and 9b, by interpolation of the measured data:  $\frac{I_m(G_i, AM, \theta, T)}{I_{m0}(1 + \alpha' \Delta T_{cell})PR_{am}PR_{aoi}}$  and

$$\frac{V_m(G_i, AM, \theta, T_0)}{V_{m0}(1 + \beta' \Delta T_{cell})}$$

The  $PR_g$  takes into account both the nonlinear dependence of the mpp voltage from the incident irradiance that becomes important at low irradiance values and the series resistance losses ( $R_s I_m^2$ ) that become important at high irradiance levels.

## 2.4. Nominal power variation

To evaluate the PR from the acquired outdoor data, it is necessary to know the module nominal power, usually using the value declared by the module manufacturer ( $P_n$ ).

Frequently this value of  $P_n$  does not correspond either to other STC laboratory measurements or to the nominal average value that can be deduced from outdoor data ( $\langle P_{m0} \rangle$ ).

Moreover, the nominal power in ROC could not always be considered constant in time:

- All the modules are subjected to a long term degradation, mainly due to aging (years).
- Some modules are subjected to initial degradation, mainly due to light soaking (days/months).
- Some module technologies are subjected to periodic seasonal variations, mainly due to the simultaneous and competitive effects of light soaking and thermal annealing (days/months).

For c-Si modules, it has been shown that a very rapid and small initial degradation could appear while no seasonal variation has been found [10].

On the contrary, in a-Si:H modules, the variation of a-Si dangling bonds amount saturated by H in the intrinsic layer, induced by light soaking and thermal annealing, causes a change of modules nominal power. Indeed, the light soaking induced initial degradation that depends on the number of junctions could reach the 30% of  $P_n$ , on a monthly time scale (Staebler–Wronsky effect). On the other hand, a partial regeneration of the degraded power, due to thermal annealing, has been proved. These degradation and regeneration phenomena produce a time variation of nominal power that contributes to the PR seasonal behavior [11,12]. How much this effect is important with respect to the others is still not clear. Recently, Friesen *et al.* [6], Nikolaeva-Dimitrova [13], and Ishii *et al.* [14] tried to estimate this effect contribution.

For these reasons, the nominal power variation effect could not always be neglected in a PR model.

By definition, it is possible to write

$$P_m(t) = P_{m0}(day)PR'(t) \frac{G_i(t)}{G_0} = P_n \left( \frac{\langle P_{m0} \rangle}{P_n} \right) \left( \frac{P_{m0}(day)}{\langle P_{m0} \rangle} \right) PR'(t) \frac{G_i(t)}{G_0} \quad (11)$$

where  $P_m(t)$  is the module produced power at time  $t$  in the specific *day*;  $P_{m0}(day)$  is the nominal power of the module measured in the specific *day*;  $PR'(t) = (PR_{am}PR_{aoi}PR_tPR_g)$  is the overall instantaneous PR that includes spectral, AOI, temperature, and irradiance effects;  $G_i(t)$  is the POA irradiance at time  $t$  in the specific *day*;  $\langle P_{m0} \rangle$  is the nominal power deduced from outdoor data (average value over the period of monitoring); and  $P_n$  is the nominal power declared by the module manufacturer.

From Equation 11, it is possible to model the nominal power variation effect by two terms, one constant and one daily dependent:

$$\Delta P_n = \frac{\langle P_{m0} \rangle}{P_n} \quad (12)$$

$$PR_s(day) = \frac{P_{m0}(day)}{\langle P_{m0} \rangle}$$

$\Delta P_n$  takes into account the nominal power variation between the one declared by the manufacturer and the stabilized power deduced from outdoor data. It includes possible mismatch in nominal power laboratory measurements and differences between nominal and stabilized power (average STC power measured over the monitoring period). This constant factor produces a constant loss that it is called “initial degradation effect.”

$PR_s(day)$  (seasonal PR) takes into account the nominal power daily variation with respect to the average STC power measured over the monitoring period. It includes fluctuations of nominal power due to light soaking degra-

ation and thermal annealing regeneration process. The loss resulting from this daily dependent factor is called “power seasonal effect” (PSE).

## 2.5. Performance ratio and losses analysis

As easily proved in [6], the PR over a period ( $d$ ) can be calculated as follows:

$$PR(d) = \frac{\sum_t PR(t)G_i(t)}{\sum_t G_i(t)} = \frac{\sum_t (PR_{am}PR_{aoi}PR_tPR_g\Delta P_nPR_s) G_i(t)}{\sum_t G_i(t)} = \frac{\sum_t (\prod_{i=1,5} PR_i) G_i(t)}{\sum_t G_i(t)}$$

$$L(d) = 1 - PR(d)$$

where  $t$  is the data sampling rate that in this case is 1 min, and  $PR_i$  is one of the five mentioned PRs:  $PR_{am}$ ,  $PR_{aoi}$ ,  $PR_t$ ,  $PR_g$ , and  $(\Delta P_nPR_s)$ , and  $L$  is the total loss. Note that negative losses are gains.

In the same way, it is possible to calculate  $PR_i(d)$  and  $L_i(d)$ . Both  $PR_i(d)$  and  $L_i(d)$  give a good indication of the impact of each single effect over the overall PR, but their values do not have a real physical meaning. Indeed, in ROC, there does not exist a period ( $d$ ) in which only a single phenomenon ( $i$ ) affects the module performance, while, in general, all the effects operate simultaneously.

However, it is clear that each  $PR_i(d)$  and  $L_i(d)$  should be related to their overall value  $PR(d)$  and  $L(d)$ . Thus, it is possible to quantify the contribution of each effect to the total loss with the reasonable hypothesis that the total loss absolute value should be proportional (through a constant  $Fr$ ) to the absolute value of average losses:

$$|L(d)| = Fr \left| \frac{\left( \sum_{i=1}^5 L_i(d) \right)}{5} \right| = Fr | \langle L_i(d) \rangle_i |$$

In this way, it is possible to define the loss fractions as

$$LF_i(d) = \frac{Fr}{5} L_i(d) \quad (14)$$

$$Fr = \frac{|L(d)|}{| \langle L_i(d) \rangle_i |}$$

Each  $LF_i$  quantifies the contribution of one effect over the total loss calculated for a period ( $d$ ). The sign of  $LF_i$  indicates if the effect brings gain (negative) or loss (positive). The absolute value of the sum is equal to the absolute value total loss:

$$\left| \sum_i LF_i(d) \right| = |L(d)|$$

Because  $\Delta P_n$  is a constant value, it should be calculated, but it does not add any information on the PR seasonal behavior. Thus, once calculated the loss fraction  $LF_{ds}$  corresponding to  $L_{ds} = (1 - \Delta P_n PR_s)$ , it is possible to define

$$LF_{\Delta P_n} = (1 - \Delta P_n)$$

$$LF_s = LF_{ds} - LF_{\Delta P_n}$$

so that  $|L(d)| = |LF_{\Delta P_n} + LF_s + LF_{am} + LF_{aoi} + LF_t + LF_g|$ .

### 3. PERFORMANCE RATIO MEASUREMENT AND MODEL'S PARAMETERS: RESULTS AND DISCUSSION

The PRs previously described are modeled through parametric functions.

In this section, the measured parameters and the comparison between the measured and calculated PRs are reported. Moreover, both for crystalline and amorphous modules, the response to each effect is discussed.

This method has been applied to data sets coming from the outdoor monitoring of two modules of different technologies: mc-Si (KC125) and a-Si/DJ (EPV50). The measurements were taken at the Ester Laboratory, University of Rome "Tor Vergata", Italy [15].

For each module, two sets of data have been used:

- almost 1 year data set coming from ROC monitoring of module with south orientation and monthly optimal tilt (each month, the module tilt has been changed to maximize the produced energy);
- 2 months data set coming from the ROC monitoring of the module on a tracker station.

Each module is connected to a MPPT, and the maximum  $I$ ,  $V$ , and  $P$  are acquired every minute while the  $I$ - $V$  curves are registered every 10 min.

Before reporting and discussing the measurement results, two important considerations on the used measurement method have to be underlined.

First of all, the used data come from three different instruments or devices: POA pyranometer, pyrheliometer, and module; so, a filtering procedure is essential to exclude incoherent measurements. Moreover, because the aim is to deduce complex functions from the acquired data, it has to be noted that also a small mismatch between the different instrument measurements could produce big errors. Thus, also the method to control these errors is very important.

The second consideration is related to the possibility to filter the data to select and measure only one effect at a time. Excluding the PSE, the main equations that are used in the procedure are as follows:

$$P_m(G_i, AM, \theta, T_{cell}) \simeq P_{m0} (PR_{am} PR_{aoi} PR_t PR_g) \left( \frac{G_i}{G_0} \right) \quad (15a)$$

$$I_{sc}(G_i, AM, \theta, T_{cell}) \simeq I_{sc0} (PR_{am} PR_{aoi} PR_t^\alpha) \left( \frac{G_i}{G_0} \right) \quad (15b)$$

Each  $PR$  is controlled by a parameter (irradiance, temperature, etc.), and to measure an effect means to select the data fixing all the other parameters to their STC values. This operation is not always possible using the ROC data; therefore, two strategies are used. To exclude an effect, it is possible to fix the control parameter in a range in which this effect is known to be negligible. The second strategy is to use the modeled effects to correct the data and then use these corrected data to measure the other effect. Nevertheless, it is better to limit the use of the latter strategy since it brings to errors propagation. For these reasons, the measurements procedure has to be executed in a specific order:

- (1) measurement of  $T_{cell}$ ;
- (2) measurement of module STC electrical and temperature parameters;
- (3) measurement of spectral effect and model parameters;
- (4) measurement of reflection effect and model parameters;
- (5) measurement of irradiance effect and model parameters;
- (6) measurement of the PSE and model parameters;

In the appendix, the filtering procedure and the measured parameters are reported.

#### 3.1. Standard test condition electrical and temperature parameters

In Table I, the outdoor measured KC125 module parameters at the Ester Laboratory are compared with the ones obtained from indoor manufacturer measurements (nominal) and from Sandia Laboratory\* outdoor measurements of the same module type and with Supsi Laboratory indoor measurements of the same monitored module.

In Table II, the outdoor measured EPV50 module parameters at the Ester Laboratory are compared with the ones obtained from indoor manufacturer measurements (nominal) of the same module type and with Sandia Laboratory\* outdoor measurements of the same kind of module (EPV40).

In Figure 1(a) and (b), the described Equation 8 is reported, both for the c-Si and a-Si modules.

For the multicrystalline module, there is a good agreement of all the parameters between the Ester measurements and the Supsi measurements (same tested module). Small differences in power and current values between specific module measurements (Ester and Supsi) and generic module model measurements (nominal and Sandia) are found.

**Table I.** Comparison of different measurements of STC electrical and thermal parameters for c-Si module: KC125.

| KC125     |      | Nominal | Sandia Laboratory | Supsi Laboratory | Ester Laboratory |
|-----------|------|---------|-------------------|------------------|------------------|
| $P_{max}$ | W    | 125     | 125               | 120              | 120.5            |
| $V_{oc}$  | V    | 21.7    | 21.70             | 22.26            | 21.90            |
| $I_{sc}$  | A    | 8       | 8.00              | 7.74             | 7.72             |
| $V_m$     | V    | 17.4    | 17.40             | 18.03            | 17.48            |
| $I_m$     | A    | 7.2     | 7.20              | 6.74             | 6.90             |
| $FF$      |      | 0.72    | 0.72              | 0.71             | 0.71             |
| $\alpha$  | %/°C | —       | 0.11              | 0.0502           | 0.07             |
| $\beta$   | %/°C | —       | -0.39             | -0.3256          | -0.36            |
| $\alpha'$ | %/°C | —       | -0.01             | —                | 0.02             |
| $\beta'$  | %/°C | —       | -0.50             | —                | -0.48            |
| $\gamma$  | %/°C | —       | -0.51             | -0.4438          | -0.47            |

STC, standard test condition.

**Table II.** Comparison of different measurements of STC electrical and thermal parameters for a-Si modules: EPV50 and EPV40.

| EPV50     |      | Nominal | Ester Laboratory | EPV40 Sandia Laboratory |
|-----------|------|---------|------------------|-------------------------|
| $P_{max}$ | W    | 50.00   | 40.74            | 40.32                   |
| $V_{oc}$  | V    | 60.00   | 58.66            | 60.96                   |
| $I_{sc}$  | A    | 1.41    | 1.29             | 1.16                    |
| $V_m$     | V    | 45.00   | 42.05            | 44.80                   |
| $I_m$     | A    | 1.12    | 0.97             | 0.90                    |
| $FF$      |      | 0.59    | 0.54             | 0.57                    |
| $\alpha$  | %/°C | 0.09    | 0.29             | 0.06                    |
| $\beta$   | %/°C | -0.28   | -0.26            | -0.32                   |
| $\alpha'$ | %/°C | —       | 0.49             | 0.11                    |
| $\beta'$  | %/°C | —       | -0.30            | -0.33                   |
| $\gamma$  | %/°C | -0.19   | 0.14             | -0.22                   |

STC, standard test condition.

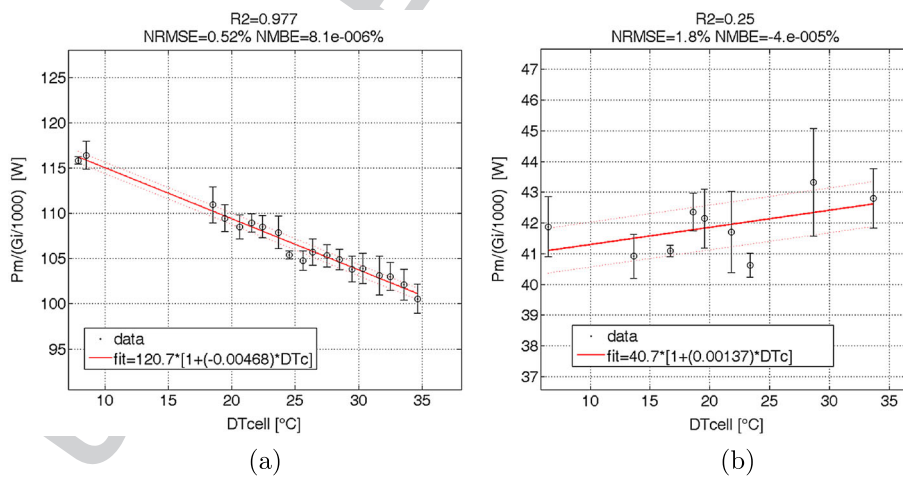


**Figure 1.** (a)  $P_m$  fit for c-Si module: KC125. (b)  $P_m$  fit for a-Si module: EPV50.

These differences could depend on module type mismatch, instrumental mismatch, and small initial degradation. An initial power degradation (mainly due to current),  $L_{\Delta P_n} = (1 - \Delta P_n) \sim 3\%$ , has been observed for this module tech-

nology [16] (where the quantity  $\Delta P_n$  has been defined in Equation 12).

For the amorphous module, big differences in power, currents, and  $\alpha$ ,  $\alpha'$ ,  $\gamma$  coefficients are found. The power and

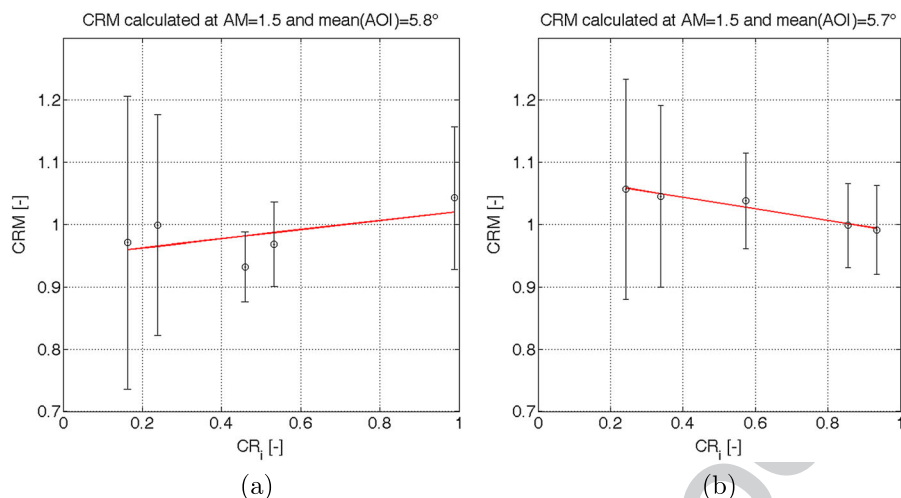


**Figure 2.** (a)  $CRM(CR_i)$  measures and fit versus  $CR_i$  for c-Si module: KC125. (b)  $CRM(CR_i)$  measures and fit versus  $CR_i$  for a-Si module: EPV50. CR, cloud ratio; CRM, CR modifier.

currents differences between the nominal and the outdoor measurements could depend mainly on the amorphous Staebler–Wronsky effect. The found initial power degradation  $L_{\Delta P_n} \sim 18\%$  is coherent with the values reported in the literature for double junction thin films.

The measured  $\alpha$ ,  $\alpha'$  coefficients are almost four times greater than the nominal and Sandia Laboratory ones so that an inversion of module power thermal response is found. Thus, a positive, instead of negative,  $\gamma$  is measured. The  $\alpha$ ,  $\alpha'$  values are no longer coherent with the literature [17,18] and seem to be physically meaningless. Nevertheless, no result could be achieved using negative  $\gamma$  coefficient, and the daily PR behavior could not be explained in terms of other effects. This apparent contradiction could be understood considering that light soaking and thermal annealing not only modify the nominal power but also cause a slow changing in the temperature module response. Such change could not be detected by instantaneous indoor or outdoor measurements that always bring to small intrinsic positive  $\alpha$ ,  $\alpha'$  and negative  $\gamma$ . Thus, ROC temperature coefficients are time dependent because they result from combined and competitive effects of intrinsic junction temperature response, light soaking, and thermal annealing. The first effect acts on an hourly time scale and could be easily measured in a laboratory. The second effect induced by light soaking and thermal annealing acts on a daily time scale, and it depends on the module history and could not be measured in a laboratory. We call such phenomenon “temperature seasonal effect.” The fact that  $\alpha$ ,  $\alpha'$ ,  $\gamma$  values depend strongly on the time period of the data confirms this explanation. Similar results have been found in [19] in which, using statistical method, the  $\gamma$  coefficient of the amorphous and crystalline modules have been measured on hourly and daily time scales.

Thus, the measured parameters well describe the module ROC temperature behavior, but they should be considered as average values over the monitoring period.

They could correspond to instantaneous measured value (as for the crystalline module) or not (as for the amorphous module). Figure 1 shows that the power versus temperature behavior is almost perfectly linear for KC125, while for EPV50, it is fluctuating around the fit average curve. In Figure 1(a) and (b), the error bar is less than  $\pm 10\%$ , but for the crystalline module, it is very small. While for the amorphous module, it is wider reflecting the time power variation.

### 3.2. Spectral effect

It is well known that in overcast days, the spectrum of the global irradiance is blue shifted with respect to the spectrum of clear days. It is also known that the spectrum of the direct irradiance is peaked on the green, and it is red shifted at high AM. On the other hand, less information is available on the spectrum of the diffuse component of irradiance. In [20], it is proved that the spectrum of the diffuse component in overcast conditions (*high*  $CR_i$ ) is less blue than the spectrum of the diffuse component in clear sky times (*low*  $CR_i$ ). The fact that the spectrum of the global irradiance in the overcast moments is more blue rich than the one of the clear sky moments depends on the overlapping of diffuse and direct spectrum. Indeed, in overcast conditions, the diffuse component is dominant resulting in a bluer global irradiance spectrum. On the contrary, in clear sky conditions, the direct component of the irradiance is dominant covering up the blue diffuse component, resulting in an overall redder global spectrum.

Figure 2 shows the dependence of the modules spectral performance from the diffuse POA spectrum variations at AM near  $AM_0$ . Such dependence is very small because the diffuse spectrum variation is small at a fixed AM.

\* <http://pvpmc.org>

Nevertheless, a different behavior between the c-Si and a-Si modules could be pointed out. The figure shows that the c-Si module exhibits better performance at high  $CR_i$  and so at redder spectrum while the a-Si module exhibits an opposite behavior.

**F3** Figure 3(a) and (b) shows the dependence of the modules spectral performance from  $AM$  and so from the average direct POA spectrum variations. As expected, the modules performance behavior is the same with the one previously pointed out. According to [4,17], the performance of c-Si grows with red shifted spectrum while the performance of a-Si decreases dramatically with the redder spectrum. The c-Si module with a small energy gap reacts very well to high infrared irradiance while the fraction of the blue wavelength irradiance, not used for electrons extraction, is dissipated into heat causing a decrease of quantum efficiency in this part of the spectrum. For the a-Si module, with greater energy gap, high infrared irradiation

is not enough to extract electron while the blue irradiance is all used for photogeneration.

Furthermore, Figure 3(b) shows that, for the a-Si double junction module, the performance decreases not only with high  $AM$  (red spectrum shift) but also with  $AM \simeq 1$ . Such small reduction at small  $AM$  is due to the mismatch between the junction photogenerated currents. Multi-junction cells spectral response is optimized for a reference spectrum, and also small variations from this spectrum result in performance losses. This is known as the secondary spectral effect (SSE) characteristic of multi-junction devices [8,21]. This secondary effect was measured for the same module by also using a spectroradiometer [9].

Figure 3(c) shows the quantum efficiency of the top and bottom cells of the EPV a-Si module. The top cell has a current density  $J_{top} = 6.65 \text{ mA/cm}^2$  while the bottom cell has a current density  $J_{bottom} = 6.01 \text{ mA/cm}^2$ ; thus,

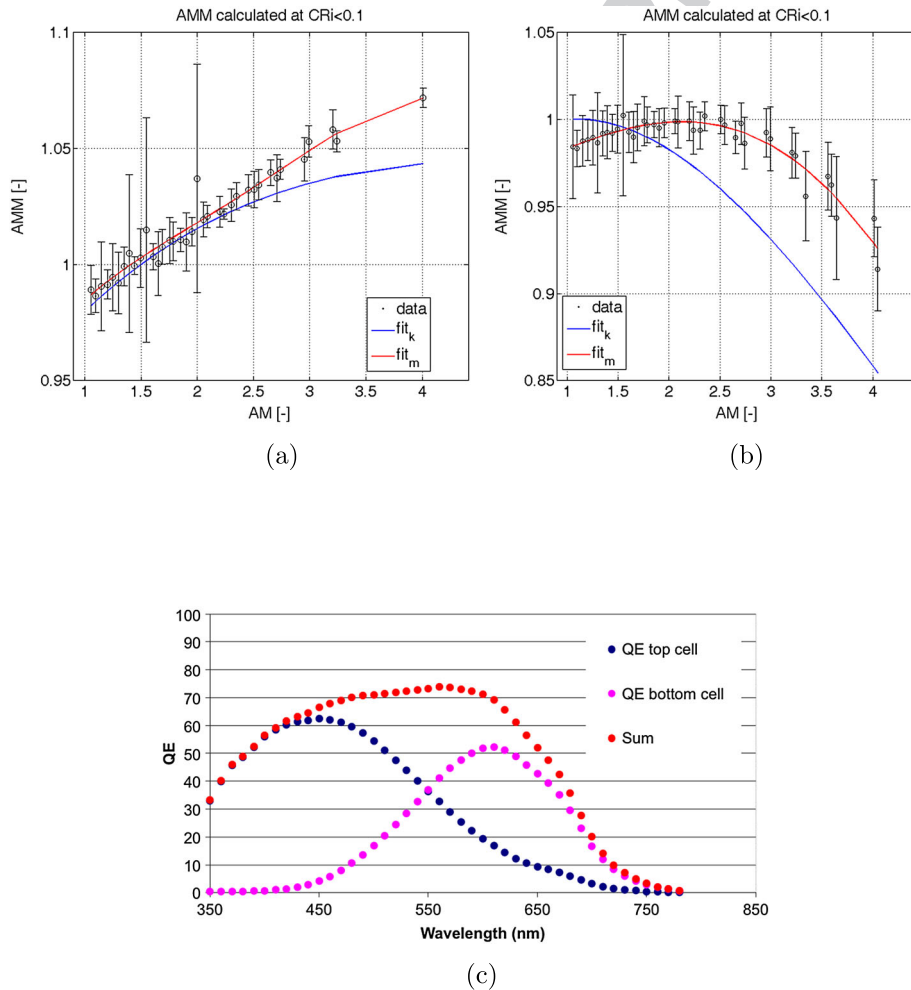


**Figure 3.** (a)  $AMM(AM)$  measures, fit ( $fit_m$ ) and fit with Sandia Laboratory coefficients ( $fit_k$ ) versus  $AM$  for c-Si module: KC125. (b)  $AMM(AM)$  measures, fit ( $fit_m$ ) and fit with Sandia Laboratory coefficients ( $fit_k$ ) versus  $AM$  for a-Si module: EPV50. (c) QE of EPV solar cell 2760-1 measured at NREL. AMM, air mass modifier.

Color Online, B&W in Print

the module is bottom limited in terms of current matching condition. This effect is amplified for bluer irradiance spectrum ( $AM < 1.5$ ) where the top cell photocurrent is even greater than the one produced by the bottom cell (SSE).

Table A.1 shows the measured parameters ( $CA - CB$ ) for  $CRM$  and  $AMM$  functions and the Sandia Laboratory parameters ( $CBk$ ) for the  $f_1$  function (described in [6]).

Finally, in Figure 3(a) and (b), the curve obtained using the Sandia Laboratory fit coefficients\* ( $fit_k$ ) is also plotted. For the crystalline module, there is a good agreement between the two fitting curves, while for the amorphous module, greater differences are found.

Unfortunately, the 2 month tracker measurements used do not contain available data with  $AM$  greater than 6, so no information on module performance could be retrieved for high air mass. Thus, the measured fitting curve ( $fit_c$ ) could not be used to model all the annual data that reach  $AM$  around 11. For this reason, in the following analysis, the Sandia Laboratory  $AMM$  coefficients are used ( $CBk$  coefficients reported in Table A.1), causing a small overestimation of a-Si spectral effect in clear sky days.

**F4** Figure 4(a) and (b) shows the modules daily behavior of the spectral performance in a clear sky day. It is possible to note that for c-Si, the  $PR_{am}$  obtained with the calculated parameters ( $CB$ ) and with the Sandia parameters ( $CBk$ ) are very similar and follow the measured spectral performance. As expected, for the a-Si module, bigger differences between the two calculated performance are found. In this case, the measured parameters for  $AMM$  function produce a better approximation of the spectral performance. It could be noted the small decrease of  $PR_{am}$  when  $AM$  is between 1 and 2 because of the SSE.

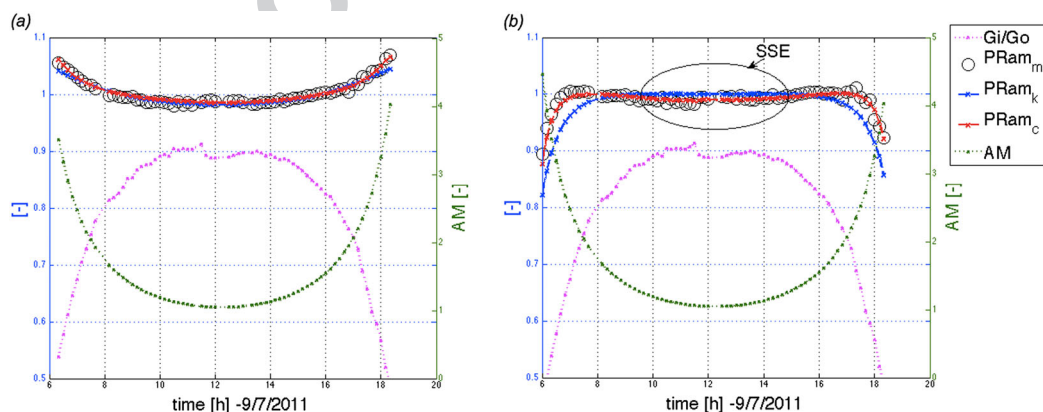
**F5** Figure 5 shows the instantaneous spectral performance behavior for the a-Si module in different day typologies characterized by different daily CR range. In this figure, the difference between the spectral performance estimated and reported in this paper (Ester model) and the Sandia model developed by King *et al.* [4] could also be found. Average  $PR_{am}$  (measured and calculated by the Ester and Sandia models), NRMSE, and NMBE between measure-

ments and calculations are reported. Because the  $AMM$  parameters used in the Sandia model are not the measured ones, a small overestimation of the spectral effect for clear sky days ( $CR \leq 0.4$ ) is found. More important is that this spectral performance model can be used in cloudy days with ( $CR > 0.4$ ), because the  $PR_{am}$  does not depend on the air mass any more, and it correctly goes to 1. Better results could be achieved using a longer period of tracker data. In any case, further investigation should be carried out to better model the spectral effect at high CR ( $CR > 0.8$ ). For these days, the broad  $PR_{am}$  scattering at  $AM$  near to one and the resulting performance under estimation are not clear. It should be underlined that the same data scattering was found in [20], where for cloudy conditions and  $AM < 4$ , a wide range of average photon energy of the diffuse irradiance was measured. So the module spectral performance reflects this wide range of the diffuse energy, while the model does not reproduce this behavior.

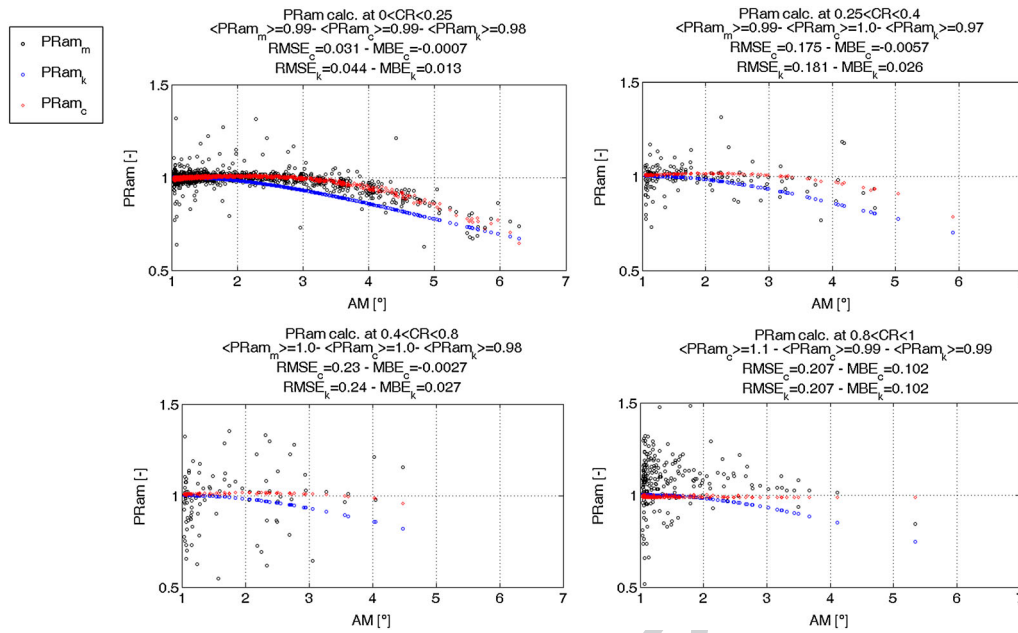
### 3.3. Reflection effect

Figure 6(a) and (b) shows the dependence of the reflection performance from the direct irradiance incidence angle. It can be seen that the reflection effect is greater for the crystalline than the amorphous module, confirming the literature [4].

In Figure 6, also the fitting curve of the acquired data ( $fit_m$ ) and the curve obtained using the Sandia Laboratory fitting coefficients ( $fit_k$ ) are reported. For the c-Si module, a small overestimation of the Sandia  $IAM(\theta)$  function with respect to the measurement is found with  $NMBE = 2.7\%$ . It could depend on soiling effect that it is greater at greater AOI [22]. On the contrary, for a-Si, a small underestimation is found with  $NMBE = -1.4\%$  that could depend on the reported a-Si underestimation of  $PR_{am}$  used in Equation 5 to correct the measured data. In any case, the error between the Sandia Laboratory fit and the measurements is very small with  $NRMSE = 4.7\%$  for the crystalline module and  $NRMSE = 4.4\%$  for the amorphous module. It must be highlighted that it is not easy to perform the



**Figure 4.** Spectral performance measured ( $PR_{am,m}$ ), calculated with Sandia Laboratory coefficients ( $PR_{am,k}$ ) and with measured coefficients ( $PR_{am,c}$ ) in a clear sky day, (a) for c-Si module: KC125 and (b) for a-Si module: EPV50. PR, performance ratio.



**Figure 5.** Spectral performance measured ( $data - PRam_m$ ), calculated with Sandia Laboratory coefficients ( $King - PRam_k$ ) and with measured coefficients ( $calc - PRam_c$ ), for a-Si module: EPV50 in four typology of days characterized by different daily cloud ratio (CR). PR, performance ratio.

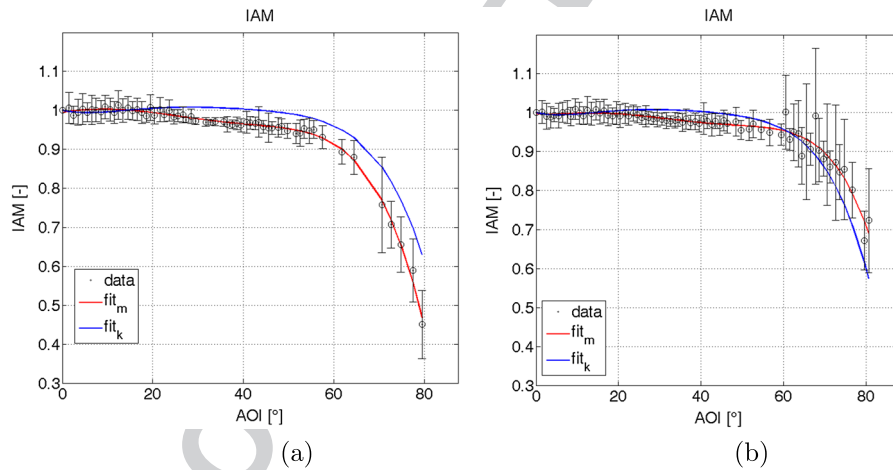


**Figure 6.** (a)  $IAM(\theta)$  measures, fit ( $fit_m$ ) and fit with Sandia Laboratory coefficients ( $fit_k$ ) versus  $\theta$  for c-Si module: KC125; (b)  $IAM(\theta)$  measures, fit ( $fit_m$ ) and fit with Sandia Laboratory coefficients ( $fit_k$ ) versus  $\theta$  for a-Si module: EPV50. IAM, incident angle modifier.

relative response measurement from outdoor fixed stand data, because the errors grow for angle greater than  $60^\circ$ . The quite good agreement between different fits ( $fit_m - fit_k$ ) proves the reliability of the reported method.

Table A.2 reports the measured parameters ( $CC$ ) and the Sandia Laboratory parameters ( $CCK$ ) for the AOI function.

**F7** Figure 7(a) and (b) shows the modules daily behavior of the reflection performance in a clear sky day. It is possible to note that for c-Si, the  $PRaoi$  obtained with the ( $CC$ ) calculated parameters ( $PRaoi_c$ ) and with the ( $CCK$ ) Sandia Laboratory parameters are very similar

although the  $PRaoi_c$  seems to give a small better estimation of measured performance ( $PRaoi_m$ ). For the a-Si module, larger differences between the calculated performance ( $PRaoi_c$  and  $PRaoi_k$ ) and the measured one ( $PRaoi_m$ ) are found. For both modules, a  $PRaoi_m$  asymmetric behavior with respect to the AOI has been observed, probably due to a not perfect south orientation of the module stand. Moreover, the increase of the a-Si  $PRaoi_m$  when the AOI is near its minimum, it is not clear. It may depend on a bad correction in temperature or spectrum of the acquired data.

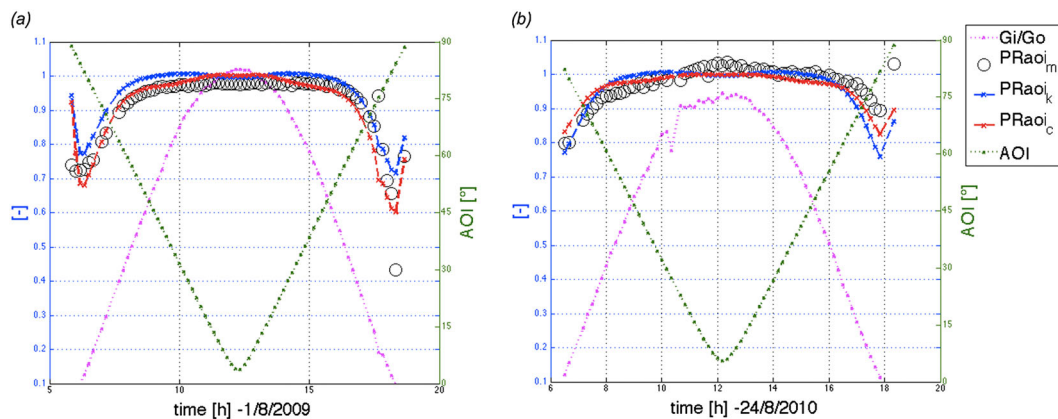


**Figure 7.** Reflection performance measured ( $PR_{aoi_m}$ ), calculated with Sandia Laboratory coefficients ( $PR_{aoi_k}$ ) and calculated with measured coefficients ( $PR_{aoi_c}$ ) in a clear sky day, (a) for c-Si module: KC125 and (b) for a-Si module: EPV50. PR, performance ratio.

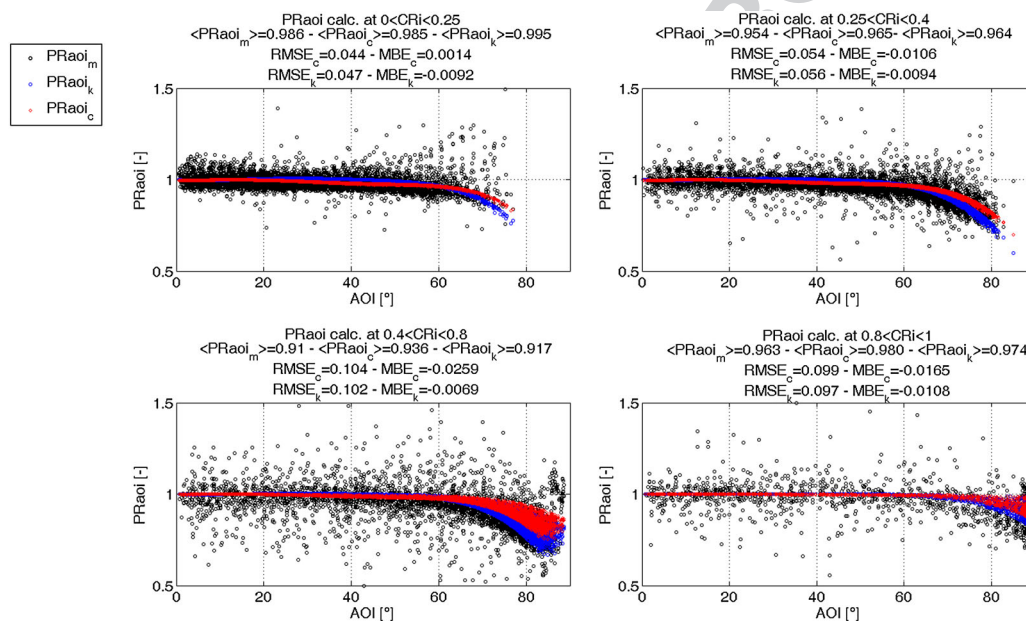


**Figure 8.** Reflection performance measured ( $data - PR_{aoi_m}$ ), calculated with Sandia Laboratory coefficients ( $King - PR_{aoi_k}$ ) and with measured coefficients ( $calc - PR_{aoi_c}$ ), for a-Si module: EPV50 in four types of days characterized by different daily cloud ratio (CR). PR, performance ratio.

**F8** Figure 8 shows the instantaneous reflection performance behavior for the a-Si module in different day typologies characterized by different daily CR range. In this figure, the difference between the performance estimated by (CC) coefficients,  $PR_{aoi_c}(calc)$ , and by (CCK) coefficients,  $PR_{aoi_k}(king)$ , could also be found. Average  $PR_{aoi}$  (measured and calculated), NRMSE, and NMBE between measurements and calculations are reported. In all the cases, there is a good agreement between measured and calculated performance. The  $PR_{aoi}$  calculated using measured parameters (CC) has a smaller RMSE for  $CR < 0.8$  while the  $PR_{aoi}$  calculated with

Sandia (CCK) parameters has a smaller RMSE for  $CR > 0.8$ . For the c-Si module, the calculated parameters work always a little bit better.

In Figure 8, it must be pointed out that the broad  $PR_{aoi}$  scattering at  $\theta \approx 90^\circ$  is exactly equal to the  $CR_i$  scattering because  $IAM(\theta) \approx 0$  and  $PR_{aoi} = CR_i$ .

### 3.4. Irradiance effect

Figure 9(a) and (b) shows the behavior of performance with respect to the POA irradiance measured at a fixed cell temperature  $T_{cell} \approx 25^\circ C$ . The scattered data at low

Color Online, B&W in Print

Color Online, B&W in Print

**F9**

Color Online, B&W in Print

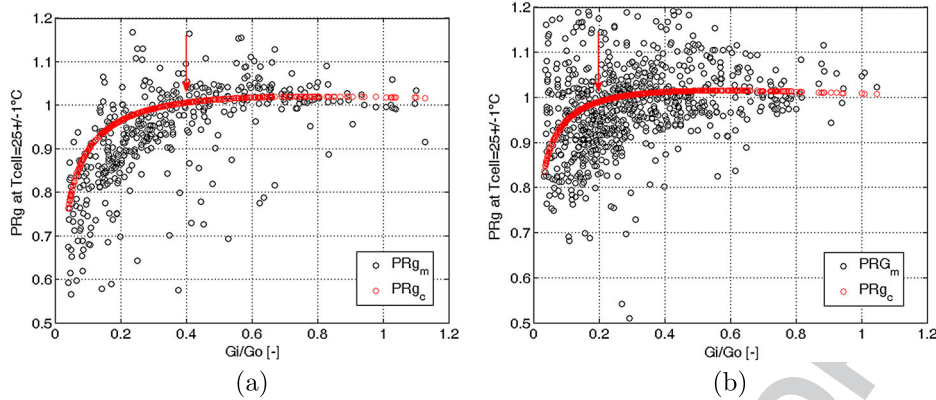


**Figure 9.** (a) Irradiance performance measured ( $PR_{g_m}$ ) and calculated ( $PR_{g_c}$ ) at fixed  $T_{bom}$  of c-Si module: KC125; (b) irradiance performance measured ( $PR_{g_m}$ ) and calculated ( $PR_{g_c}$ ) at fixed  $T_{bom}$  of a-Si module: EPV50. PR, performance ratio.

**Table III.** PR and losses over the monitored period.

|                   | KC125 (%) | EPV50 (%) |
|-------------------|-----------|-----------|
| $PR_m$            | 88.3      | 84.4      |
| $L_m$             | 11.7      | 15.6      |
| $PR_c$            | 88.6      | 84.6      |
| $L_c$             | 11.4      | 15.4      |
| $LF_{\Delta P_n}$ | 3.44      | 18.52     |
| $LF_s$            | —         | 0.18      |
| $LF_t$            | 7.38      | -2.59     |
| $LF_{am}$         | 0.42      | -0.36     |
| $LF_{aoi}$        | 1.63      | 1.23      |
| $LF_g$            | -1.43     | -1.57     |

PR, performance ratio.

irradiance are mainly due to irradiance instability and, for the a-Si module, to the high sensitivity to temperature, spectral, and reflection corrections. The fitting model is not performing well at low irradiance level, and further research should be performed. However, for the crystalline module, this model gives the best result with respect to the others tested, improving the correlation between the daily measured and calculated PRs by 10%. On the other hand, it has been observed that small variations of temperature, spectral, and reflection corrections could lead to small variation of the current fitting coefficient ( $C_3 = 1 \pm 0.001$ ; Equation 10) resulting either in small daily gain or loss ( $LF_g = -/+ 1\%$ ). Thus, for this kind of amorphous module, the model results are not reliable, and the estimated loss fraction will not be discussed in the next section.

However, from the figures, it emerges that for the crystalline module under test, a sensible decrease of the measured  $PR_g$  around  $400 \text{ W/m}^2$  can be observed, while for the amorphous module, the data are too scattered for any further consideration.

**T3** Table A.3 reports the measured parameters ( $C$ ) for the  $PR_g$ .

### 3.5. Power seasonal effect

In [6], to estimate the seasonal variation of the nominal power, indoor measurements of module STC power in different days of the monitored period have been performed.

Unfortunately, in this work, it is not possible to use this method because no indoor laboratory is available; thus, a method to model the PSE from only outdoor long period data is developed. The main reasonable hypothesis is that light soaking and thermal annealing affect the nominal power ( $P_{m0}(day)$ ) and the power ( $P_m^c(day)$ ) produced at  $T_{cell} = T_1 \neq T_0$ ,  $AM$  near  $AM_0$ ,  $\theta$  near  $\theta_0$ , and  $G_i$  near  $G_0$ , so that

$$PR_s(day) = \frac{P_{m0}(day)}{\langle P_{m0} \rangle_{mp}} \simeq \frac{P_m^c(day)}{\langle P_m^c \rangle_{mp}}$$

$$P_m^c(day) = \left\langle \frac{P_m(G_i, T_1, AM_0, \theta_0)}{(G_i/G_0)} \right\rangle_{day}$$

The seasonal performance is approximated by a fourth degree polynomial function of time (days):  $PR_s = \frac{P_m^c(day)}{\langle P_m^c \rangle_{mp}} \simeq \sum_{n=0}^4 CS_n (days)^n$ .

As expected, for the crystalline module, no appreciable daily power variation is found.

Figure 10 shows the agreement between the a-Si module measured and the modeled daily PR (from 1 November 2009 to 31 October 2010), considering and not considering the seasonal effect.

It can be seen that, excluding the  $PR_s$  contribution, the performance time behavior is not well reproduced by the model with a correlation coefficient (between measured and calculated data)  $Corr = 32\%$ . Introducing in the model the seasonal performance, the agreement between measurements and calculations is greatly improved with  $Corr = 67\%$ . As discussed in the next section, the measured  $PR_s$  agrees with other laboratory measurements.

Color Online, B&W in Print

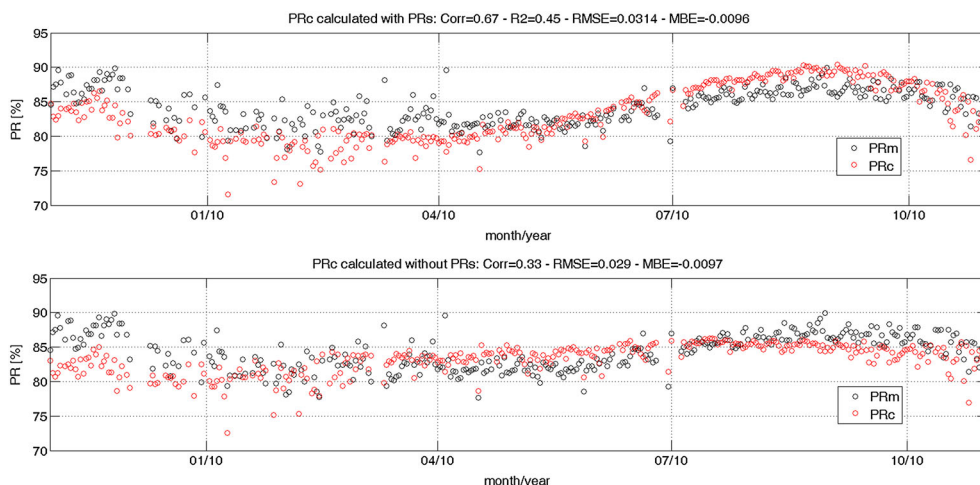


**Figure 10.** Comparison between a-Si performance ratio measured ( $PR_m$ ) and calculated ( $PR_c$ ) considering and not considering the seasonal performance ( $PR_s$ ). PR, performance ratio.

It has to be remarked that to measure  $PR_s$ , no correction coefficients are used. The  $G_i$ ,  $AOI$  and  $AM$  are fixed in the range in which the related effects are quite small. Besides, the  $PR_s$  trend cannot be affected from the module temperature response because it has been measured at a fixed  $T_{bom}$ . It has been found that the  $PR_s$  strongly depends on the number of  $P_m^c(day)$  measurements used for the interpolation. On the other hand, it does not depend too much from the range of  $G_i$ ,  $AOI$ , and  $AM$ ; in this case, to improve the statistic, the range has been fixed between  $\{600 \text{ W/m}^2; 1200 \text{ W/m}^2\}$ ,  $\{0^\circ; 35^\circ\}$ , and  $\{1; 2.5\}$ .

As it is shown in [6,14,23] and [13], also in this case, the seasonal performance ( $PR_s$ ) could not be neglected to achieve a reliable characterization of the amorphous thin film seasonal behavior.

#### 4. SEASONAL BEHAVIOR ANALYSIS

Table III reports, for both the c-Si and a-Si modules, the PR and losses (measured and calculated) over 1 year monitoring periods: 1 November 2009 to 31 December 2009 for the crystalline module and 1 November 2009 to 31 October 2010 for the amorphous module. Also the losses fractions as defined in Equation 14 are calculated.

As expected, for the crystalline technology, the greater contribution to the overall losses results from the temperature effect ( $LF_t = 7\%$ ) followed by initial decay loss ( $LF_{\Delta P_n} = 3.4\%$ ). Except for the irradiance effect, all the other effects produce losses. For the tested amorphous technology, the greater loss is the initial decay ( $LF_{\Delta P_n} = 18.5\%$ ) because a big difference between

Color Online, B&W in Print

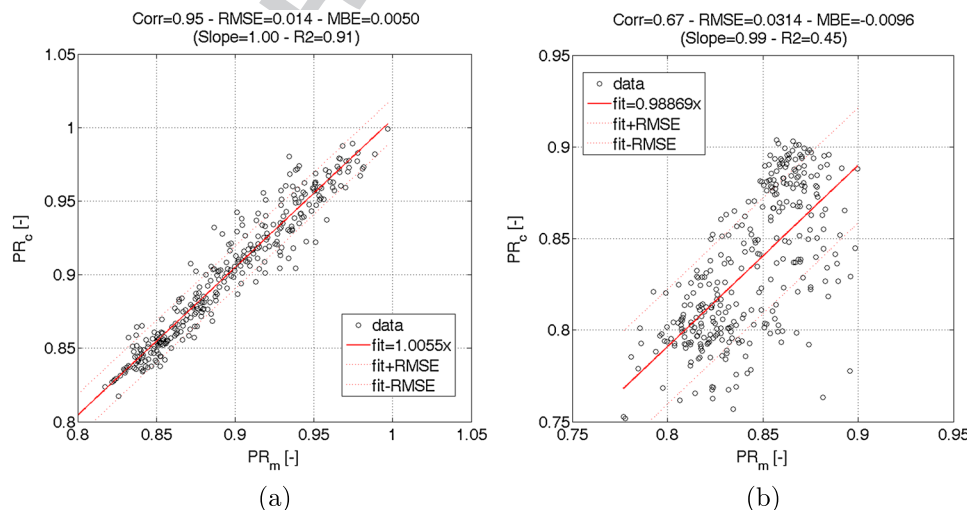


**Figure 11.** Performance ratio (PR) calculated versus measured: (a) for c-Si module: KC125 and (b) for a-Si module: EPV50.

the nominal power declared by the manufacturer and the average nominal power in ROC (reported in Table III) is found. All the other effects have a relative small impact on the annual losses. Temperature, spectral, and irradiance result in gains while power seasonal and reflection are losses. Moreover, not considering the initial degradation, the a-Si module exhibits yearly negative losses (gains) while the annual losses of c-Si module are always positive.

It should be remarked that, for both modules, reflection effect has a very small impact because the tilt angle has been changed every month of the monitoring period to optimize the energy production. This allows to measure

the incident angle relative response from outdoor data but obviously minimizes the reflection effect.

Figure 11(a) and (b) shows the calculated versus measured daily PR. For the c-Si module, there is a very good agreement correlation coefficient  $Corr = 95\%$ . For the a-Si module, a not so good result is achieved with a correlation coefficient  $Corr = 67\%$ ; however, the model seems to reproduce quite well the experimental measurements and thus can be usefully employed for losses analysis.

Figure 12(a) shows the PR and losses daily behavior of the crystalline module.

For the crystalline module, once again, it appears that the PR time trend is driven by the temperature effect

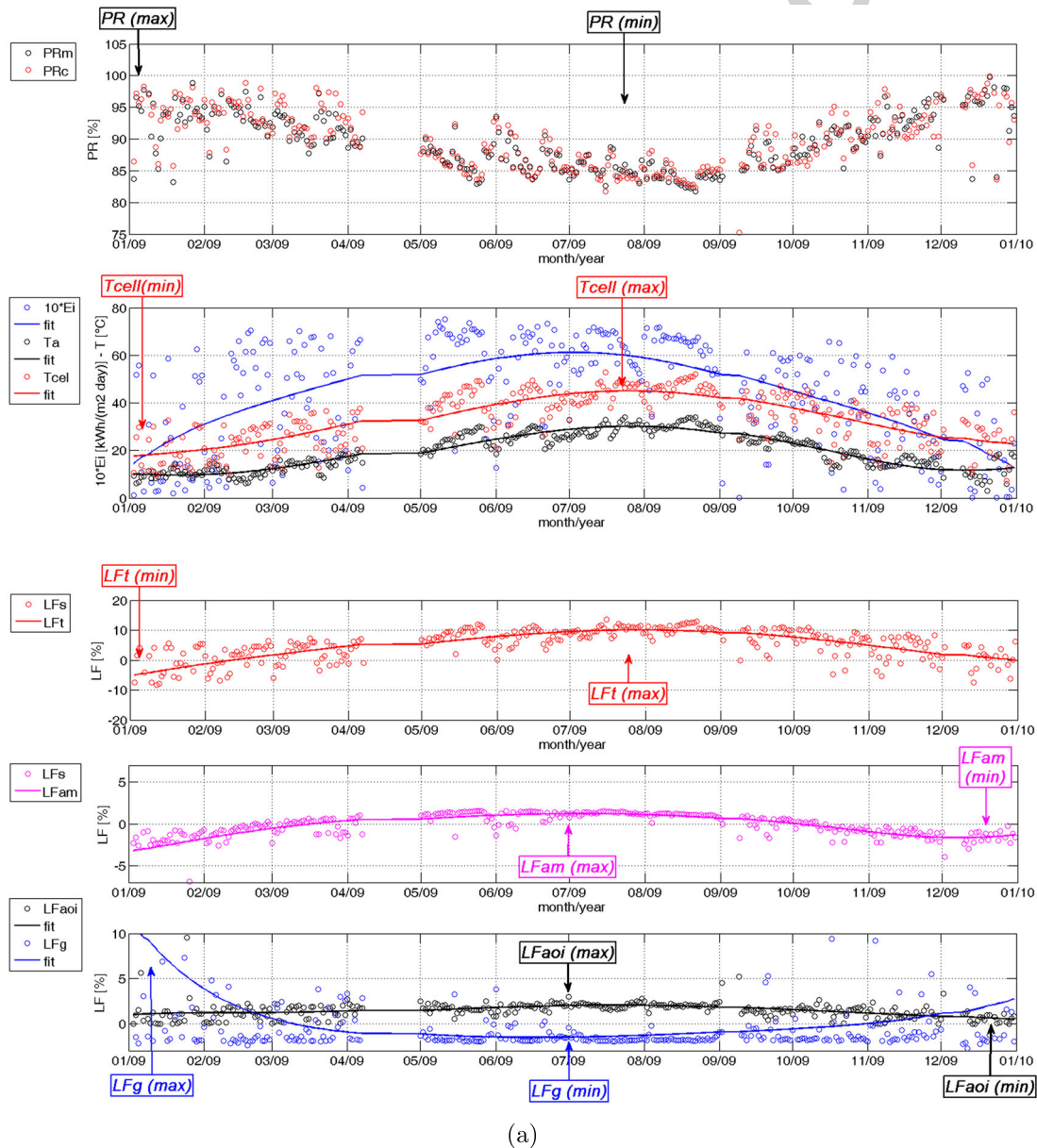


Figure 12. (a) Daily values of performance ratio (PR), radiation, temperatures, and losses for c-Si module: KC125.

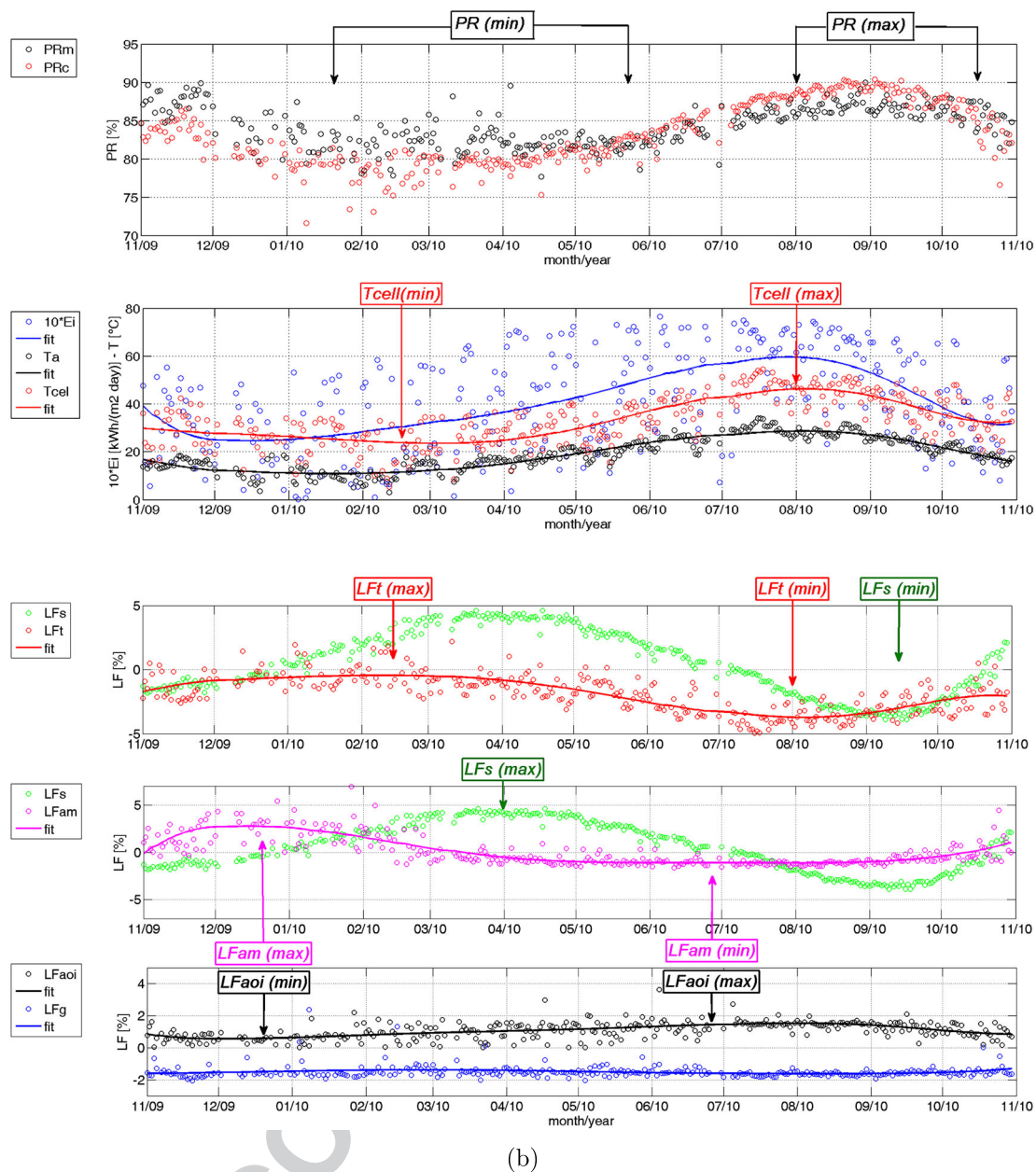


Figure 12. (b) Daily values of PR, radiation, temperatures, and losses for a-Si module: EPV50.

so that the PR minimum and maximum corresponds to the  $T_{cell}$  and Lt maximum and minimum. This effect, in Rome climatic situations, brings to a maximum of 10% loss in summer and a minimum of 5% gain in winter. Spectral and reflection effects have smaller annual fluctuation around 3% and 1% and realize their maximum in July (bluer spectrum and greater angles of incidence) and minimum in December (redder spectrum and smaller angles of incidence). Irradiance effect results in gain in clear sky days, and quite big loss in overcast days, raising up to 5% for winter days with irradiation less than  $0.8 \text{ kWh/m}^2 \text{ day}$ .

Because in the crystalline module all the effects are almost in phase, great loss in summer and gains in winter, the annual overall PR fluctuation reaches 15% amplitude.

Figure 12(b) shows the PR and losses daily behavior of the amorphous module.

For the amorphous module, in Rome climatic conditions, the temperature effect generally results in gain. It realizes the maximum loss in winter and the minimum in summer with a fluctuation of 4% amplitude. The spectral effect, in spite of the small annual impact, has a fluctuation of around 4%, according to [14], with a minimum in summer and a maximum in winter. Power seasonal effect

is minimum in September (maximum of thermal annealing power regeneration) while reaches the relative maximum around the end of March. The same result is found in Ispra [13], while in Lugano, the minimum is found in August and the maximum around February [6]. The difference between the relative maximum and minimum is around 4%. As expected, reflection effects have a very small impact. It has the same behavior as the crystalline module with a 0.5% annual variation between summer and winter.

On the whole, in the amorphous technology, the competitive impacts of spectral, power seasonal, and temperature effects produce small yearly PR fluctuations around 10%.

For what concerns reflection effects, no relevant PR differences between the two technologies can be pointed out. Nevertheless, reflection response is found; thus, for other installation features, also this effect could have a greater impact on the overall losses.

## 5. CONCLUSION

The presented parametric model reproduces the PR measurements with a satisfying level of accuracy for both crystalline and amorphous monitored modules. A correlation between measured and calculated daily PR of 95% for c-Si and 67% for a-Si was reached. This model allows to estimate and analyze separately all the effects that influence the PV performance, providing a full characterization of the module behavior in ROC. Thus, the seasonal time trends of performance are explained in terms of impact of each phenomenon.

For the temperature effect, according to the data sheet and other measurements, negative temperature coefficients are found for the crystalline module. On the contrary, for the amorphous module, the present measurement procedure brings positive power temperature coefficients. Although they well reproduce the module thermal behavior, no agreement is found with data sheet and other coefficients measurements. This is explained in terms of the combined and competitive effects of intrinsic junction negative coefficients, light soaking, and thermal annealing that modify the module temperature response [11]. Such phenomenon cannot be detected by fast indoor or outdoor measurements. The temperature coefficients estimated by the used outdoor measurement method should be considered as an average value over the monitored period and can no more be compared with the data sheet. On the other hand, the data sheet temperature parameters do not reflect the annual thermal response of the module, and no reliable results using such coefficients could be achieved.

For the spectral effect, a modification of the Sandia model is proposed [4], and the response to direct and diffuse irradiance is studied separately. This model allows to estimate the spectral effect also in cloudy conditions, and thus, the spectral effect could be evaluated for all the monitored days. On the other hand, it appears that

the spectral effect in overcast days results in gains, and it is underestimated. However, the found spectral behavior agrees in principle with other laboratories measurements. It should be remarked that the proposed model for the spectral effect is a simplified approach. It has the advantage that no spectral measurements should be performed. The crystalline module is found to be more efficient in prevalent red spectrum while the amorphous module in prevalent blue spectrum. For the double junction a-Si module, the SSE due to the mismatch between the junctions currents (bottom limitation) has been also observed.

For what concerns the reflection effects, the measured model parameters and the found results are coherent with the literature. The crystalline module is more affected by these phenomena than the amorphous thin film. For the c-Si module, the performance falls down with angles of incidence above 60°, while for the amorphous thin film, it happens for angles of incidence above 70°.

For the PSE, the difference between the relative maximum and minimum is around 4%.

For the reporting site (Rome) and installation features (open rack, south orientation, and monthly optimized tilt), the seasonal performance behavior of the crystalline module is driven by the temperature effect that reaches a daily loss peak above 10% and causes a 7% yearly loss. Small initial power degradation, small irradiance, and reflection losses are found, while the spectral loss is negligible.

For the amorphous thin film, the seasonal behavior is totally different. Even if only the initial degradation and the temperature effect produce relevant annual loss (18%) and gain (-2.6%), also spectral and PSEs could produce great daily loss or gain.

On the whole, in the amorphous technology, the competitive impacts of these three effects produce a small yearly PR fluctuation of around 10%. For the crystalline technology, the temperature, spectral, and reflection effects are in phase, and they produce a great annual fluctuation of 15%. Moreover, not considering the initial degradation, the a-Si module exhibits yearly negative losses (gains) while the annual losses of c-Si module are always positive.

Taking into account that the amorphous thin film has a lower nominal efficiency and it has a higher initial power degradation, this technology seems more suitable for BIPV plants in cloudy or hot sites while crystalline for open rack installation in sunny and cold locations.

## ACKNOWLEDGEMENTS

This work was supported by the Lazio Region within the frame of the Centre for Hybrid and Organic Solar Energy (CHOSE). The authors are supported in the frame of the research project no. 21 ("DSP Project") funded by an agreement between the Italian Ministry of Economic Development (MISE), the Italian Trade Promotion Agency (ICE), and the Conference of the Deans of the Italian Universities (CRUI).

## REFERENCES

- 01  
02  
03  
04  
05  
06  
07  
08  
09  
10  
11  
12  
13  
14  
15  
16  
17  
18  
19  
20  
21  
22  
23  
24  
25  
26  
27  
28  
29  
30  
31  
32  
33  
34  
35  
36  
37  
38  
39  
40  
41  
42  
43  
44  
45  
46  
47  
48  
49  
50  
51  
52  
53  
54  
55  
56  
57  
58
1. Skoplaki E, Palyvos JA. On temperature dependence of photovoltaic module electrical performance: a review of efficiency/power correlations. *Journal of Solar Energy Engineering* 2009; **83**: 614–624.
- AQ23 2. Friesen G, Gottschalg R, Beyer HG, Williams S, Guerin de Montgareuil A, Van der Borg N, Van Sark WJHM, Huld T, Müller B, De Keizer AC, Niu Y. Intercomparison of different energy prediction methods within the european project “performance” results of the 1st round robin, In *22th European Photovoltaic Solar Energy Conference and Exhibition*, Milano, 2007.
3. King D, Boyson W, Kratochvil J. Photovoltaic array performance model, Sandia Report SAND2004-3535 Sandia national Laboratories, December 2004.
4. King DL, Kratochvil JA, Boyson WE. Field experience with a new performance characterizations procedure for photovoltaic arrays, In *2nd World Conference and Exhibition on Photovoltaic Solar Energy Conversion*, Vienna, Austria, 1998.
5. King D, Kratochvil JA, Boyson WE. Measuring solar spectral and angle-of-incidence effects on photovoltaic modules and solar irradiance sensors, In *26th IEEE Photovoltaic Specialists Conference*, Anaheim, California, September 29–October 3, 1997.
6. Fanni L, Virtuani A, Chianese D. A detailed analysis of gain and losses of a fully integrated flat roof amorphous silicon photovoltaic plant. *Solar Energy* 2011; **85**: 2360–2373.
7. Gottschalg R, del Cueto JA, Betts TR, Infield DG. Seasonal performance of ASi single and multi junction modules in two locations, In *Proceedings of the 31st IEEE PV Specialists Conference*, Buena Vista (FL), January 3-7, 2005.
- AQ24 8. Beyer HG, Gottschalg R, Betts TR, Infield DG. Modelling the realistic short circuit current and MPP power of A-SI single and multijunction devices, In *Proceedings of the 7th Photovoltaic Science, Applications and Technology Conference*, 2003. ISBN: 4-9901816-3-8.
9. Cornaro C, Andreotti A. Influence of average photon energy index on solar irradiance characteristics and outdoor performance of PV modules, In *Progress in Photovoltaic: Research and Applications*. ISSN: 1062-7995, DOI: 10.1002/pip.2194, 2012
10. Cereghetti N, Realini A, Chianese D, Rezzonico S. Power and energy production of PV modules, In *Proceedings of 3rd World Conference on Photovoltaic Energy Conversion*, Vol. 2, 18 May 2003; 1919–1922.
- AQ25  
AQ26 11. Luque A, Hegedus S. *Handbook of Photovoltaic Science and Engineering* Lunque A, Hegedus S (eds). [12.1.3], Wiley, 2011. 511–512.
12. Wronski C. *Thin Film Hydrogenated Silicon (Si:H) Solar Cells*. SOLAR TR-1: Ankara, Turkey, April 29-30, 2010.
13. Nikolaeva-Dimitrova M, Robert K, Ewan D. Controlled conditioning of a-Si:H thin film modules for efficiency prediction. *Thin Solid Films* 2008; **516**: 6902–6906.
14. Virtuani A, Fanni L. *Seasonal power fluctuations of amorphous silicon thin-film solar modules: distinguishing between different contributions*, 2012. Progress in Photovoltaics: Research and Applications, Published online in Wiley Online Library DOI:10.1002/pip.2257
15. Spina A, Cornaro C, Serafini S. Outdoor ESTER test facility for advanced technologies PV modules, In *Proceedings of the 33rd IEEE PV Specialists Conference*, San Diego (CA), May 11-16 2008.
16. Chianese D, Friesen G, Pasinelli P, Paola D, Realini A, Cereghetti N, Bernasconi A. Direct performance comparison of PV modules, In *Proceedings of 22nd EPVSEC*, Milano, September 2007.
17. King DL, Kratochvil JA, Boyson WE. Stabilization and performance characteristics of commercial amorphous-silicon PV modules, In *Proceeding of the 28th IEEE PVSC Anchorage USA*, September 2000; 1446–1449.
18. King D, Boyson W, Kratochvil JA. Temperature coefficients for PV modules and arrays: measurement methods, difficulties, and results, In *26th IEEE Photovoltaic Specialists Conference*, Anaheim, CA, November 1997.
19. Ishii T, Otani K, Takashima T, Kawai S. Estimation of the maximum power temperature coefficients of PV modules at different time scales. *Solar Energy Materials & Solar Cells* 2011; **95**: 386–389.
20. Usami A, Kawasaki N. Modeling of solar spectra irradiance data from cloudless to overcast skies. *Japanese Journal of Applied Physics* 2012, 51 10NF06.
21. Williams SR, Beyer HG, Gottschalg R, Betts TR, Infield DG. Modelling long-term module performance based on realistic reporting conditions with consideration to spectral effects, In *Proceedings of 3rd World Conference on Photovoltaic Energy Conversion, 1908-1911*, Vol. 2, 18 May 2003.
22. Zorilla-Casanova J, Piliouguine M, Carretero J, Bernaola-Galván P, Carpena P, Mora-López L, Sidrach-de-Cardona M. *Losses produced by soiling in the incoming radiation to photovoltaic modules*, 2012. Progress in Photovoltaics: Research and Applications, Published online in Wiley Online Library DOI:10.1002/pip.1258
23. Gottschalg R, del Cueto J, Betts TR, Williams SR, Infield DG. Investigating the seasonal performance
- 59  
60  
61  
62  
63  
64  
65  
66  
67  
68  
69  
70  
71  
72  
73  
74  
75  
76  
77  
78  
79  
80  
81  
82  
83  
84  
85  
86  
87  
88  
89  
90  
91  
92  
93  
94  
95  
96  
97  
98  
99  
100  
101  
102  
103  
104  
105  
106  
107  
108  
109  
110  
111  
112  
113  
114  
115  
116

of amorphous silicon single and multi-junction modules, In *Proceedings of the 7th Photovoltaic Science, Applications and Technology Conference*, 2003. ISBN: 4-9901816-3-8.

AQ28 24. Gottschalg R, Betts TR, Infield DG, Kearney MJ. The effect of spectral variations on the performance parameters of single and double junction amorphous silicon solar cells. *Solar Energy Materials & Solar Cells* 2005; **85**: 415–428.

25. Martin N, Ruiz JM. Calculation of PV modules angular losses under field conditions by means of analytic model. *Solar Energy Materials and Solar Cells* 2001; **70**: 25–38.

26. Hunter A, Davis W, Dougherty P, King D, Boyson W, Kratochvil J. Comparison of photovoltaic module performance measurements. *Journal of Solar Energy Engineering* 2006.

## APPENDIX A

### A.1. Data filtering procedure

First of all, the data are filtered excluding measuring errors that correspond to physical meaningless values of the main variable used:  $G_i, G_i^{dni}, T_{bom}, \theta, AM$ .

Then, two main conditions are applied:

- (1) The coherence between the measurements of the plane of array (POA) pyranometer and the module production is verified by the following relation:

$$\left| \frac{I_{sc}}{G_i} - \left\langle \frac{I_{sc}}{G_i} \right\rangle \right| \leq STD \left( \frac{I_{sc}}{G_i} \right) \quad (A.1)$$

where  $\left\langle \frac{I_{sc}}{G_i} \right\rangle$  and  $STD \left( \frac{I_{sc}}{G_i} \right)$  are the mean value and the standard deviation of  $\left( \frac{I_{sc}}{G_i} \right)$ . In this way, big measurements mismatch, shadowing, and reflection effect are excluded.

- (2) A reasonable coherence between the measurements of the POA pyranometer and pyrheliometer is checked out by the condition:

$$ErrG_i = \frac{|G_i - G_i^c|}{G_i} \leq 0.2 \quad (A.2)$$

where  $G_i$  is the POA pyranometer irradiance measured value;  $G_i^c$  is the calculated POA global irradiance value:

$$G_i^c = G^{dni} \cos(\theta) + G_h^{diff} \left[ \frac{1 + \cos(\text{tilt})}{2} \right] + G^{refl} \left[ \frac{1 - \cos(\text{tilt})}{2} \right] \quad (A.3)$$

with  $G^{dni}$  is the pyrheliometer DNI measured value;  $G_h^{diff}$  is the measured diffuse irradiance (on the horizontal plane);  $G^{refl}$  is the albedo measured irradiance value.

## A.2. Measured parameters tables

**Table A.1.** Measured parameters (CA – CB) and Sandia Laboratory parameters (CBk) for the calculation of the CRM and AMM functions.

| CA (KC125) | CB (KC125) | CBk (KC125) |
|------------|------------|-------------|
| 0.9483     | 0.9122     | 0.9219      |
| 7.235 E-2  | 0.1160     | 7.089 E-2   |
|            | -5.887 E-2 | -1.427 E-2  |
|            | 1.712 E-2  | 1.171 E-3   |
|            | -1.802 E-3 | -3.371 E-5  |
| CA (EPV50) | CB (EPV50) | CBk (EPV40) |
| 1.0719     | 0.9624     | 0.9675      |
| -6.665 E-2 | 1.178 E-2  | 6.301 E-2   |
|            | 1.449 E-2  | -3.368 E-2  |
|            | -6.085 E-3 | 3.141 E-3   |
|            | 3.417 E-4  | -9.211 E-5  |

CRM, cloud ratio modifier; AMM, air mass modifier.

**Table A.2.** Measured parameters (CC) and Sandia Laboratory parameters (CCK) for the calculation of the IAM function.

| CC (KC125) | CCK (KC125) | CC (EPV50) | CCK (EPV40) |
|------------|-------------|------------|-------------|
| 0.9968     | 1           | 1.001      | 1           |
| 2.365 E-3  | -2.438 E-3  | 1.9323 E-4 | -2.438 E-3  |
| -1.201 E-4 | 3.103 E-4   | 6.576 E-5  | 3.103 E-4   |
| -1.121 E-6 | -1.246 E-5  | -5.963 E-6 | -1.246 E-5  |
| 9.485 E-8  | 2.112 E-7   | 1.403 E-7  | 2.112 E-7   |
| -1.004 E-9 | -1.359 E-9  | -1.034 E-9 | -1.359 E-9  |

IAM, incident angle modifier.

**Table A.3.** Measured parameters (C) for the calculation of the irradiance effect function.

| C (KC125)  | C (EPV50)  |
|------------|------------|
| -9.116 E-3 | -3.077 E-2 |
| -6.060 E-2 | -2.802 E-2 |
| 1.0212     | 1.0118     |

**Table A.4.** Measured parameters (CS) for the calculation of the power seasonal effect function.

| CS (EPV50)  |
|-------------|
| 1.02        |
| 2.14 E-3    |
| -1.709 E-5  |
| 1.129 E-7   |
| -1.973 E-10 |